HEFAT2012
9th International Conference on Heat Transfer, Fluid Mechanics and Thermodynamics
16 – 18 July 2012
Malta

MULTI-PHASE FLUID BEHAVIOUR AND THERMAL CHARACTERISTICS IN FLOW THROUGH HEATED CURVED DUCTS

Chandratilleke Tilak T.*,Nadim N. and Narayanaswamy R.
*Author for correspondence
Department of Mechanical Engineering,
Curtin University,
Perth WA6845,
Australia,
E-mail: t.chandratilleke@curtin.edu.au

ABSTRACT

Fluid flow and thermal characteristics in curved ducts are influenced by the secondary flow effects arising from duct curvature and are uniquely different to those in straight ducts. Such flows stimulate fluid mixing to promote wall heat transfer even in laminar flow and exhibit hydrodynamic instability under certain flow conditions. This paper provides an overview of the present knowledge-base in the field for analysing and designing technological systems with embedded curved flow geometries. It then discusses the details and outcomes of a research programme covering both single and two-phase flow behaviour in curved ducts.

As a key contribution to the field, the study develops and validates a novel numerical process based on three-dimensional vortex structures (helicity) and a curvilinear mesh system that overcomes previous modelling limitations. For both single and two-phase flow situations, computations are performed to examine the flow characteristics within rectangular, elliptical and curved ducts and, to recognise parametric influences. These are effectively deployed for physical interpretation and illustration of unique features in single and two-phase flow processes within curved ducts. The study introduces a unified approach for identifying the onset of secondary flow instability directly within the computational process. An entropy-based analysis is appraised in the study for optimising curved duct thermal characteristics.

INTRODUCTION

Curved fluid flow passages are common geometrical features in most technological systems involving fluid transport and heat exchange such as, compact heat exchangers, boilers, gas turbines blades, air conditioning and rocket engine coolant systems. The fluid motion through curved passages is uniquely different to those in straight ducts because of the centrifugal action arising from the passage curvature that affects the flow behaviour and thermal characteristics.

The centrifugal action essentially produces two key effects in the flow within curved ducts. It induces in the axial flow a lateral fluid movement directed from inner duct wall towards the outer wall, thus creating a spiralling fluid motion through the duct. This lateral fluid movement is referred to as secondary flow and is manifested by large-scale counter rotating pairs of vortices in the duct cross section. The centrifugal action also forms in the fluid flow a positive radial fluid pressure gradient towards the outer duct wall. The lateral fluid circulation takes place in this adverse pressure field and is dampened by the viscous effects to create a stagnant fluid region near the outer wall. Beyond a certain critical axial flow rate, the radial pressure gradient within the outer wall stagnant fluid region triggers a localised flow circulation to form additional pairs of counter-rotating vortices. This flow condition is commonly referred to as Dean's Instability [1] and the additional vortices are known as Dean vortices. In his pioneering work, Dean [1] identified the dimensionless term Dean Number $K = \left[\frac{D_h}{R}\right]^{\frac{1}{2}} Re$ for characterising the secondary flow behaviour.

Moffat [2] and Eustice [3] have experimentally observed and verified the critical velocity requirements for Dean's instability, while Baylis [4] and Humphery et al [5] confirmed the Dean Number to be the parameter determining secondary flow behaviour and Dean Instability. However, subsequent studies by Cheng et al [6], Ghia and Shokhey [7], and Sugiyama et al [8] showed that the duct aspect ratio and curvature ratio also influence Dean Instability in curved rectangular ducts in addition to Dean Number.

Chandratilleke et al [9,10,11] report a parametric study that extensively examined the effects of aspect ratio and curvature ratio along with the wall heat flux. They developed effectively a two-dimensional simulation model based on stream function approach with dynamic similarity in axial direction and using toroidal coordinates that was validated and well correlated with their own experimental data [10,11]. Intersecting stream function contours were deployed as a qualitative criterion for identifying the onset of Dean vortices and Dean's instability.

They discussed results in a comprehensive range of Dean number $25 \leq K \leq 500$, aspect ratio $1 \leq Ar \leq 8$ and Grashof number $12.5 \leq Gr \leq 12500$. It was illustrated that, the onset of Dean instability would strongly influenced by the duct aspect ratio and curvature ratio while the wall heat flux radically changed the flow patterns. Subsequent research by Yanase [12] and Fellouah et al [13,14] have validated the results of Chandratilleke et al [11].

The stream function approach is clearly adequate for two-dimensional flow systems, but cannot be extended for practical flow situations. Guo et al [15] used a laminar incompressible three-dimensional numerical model to explore the interactive effects of geometrical and flow parameter on heat transfer and pressure drop. They used flow entropy generation as a hydrothermal criterion and reported the influence of Reynolds number and curvature ratio on the flow profile and Nusselt number. In modelling curved rectangular ducts, Ko et al [16] proposed a technique of splitting the overall flow entropy into separate contributions from flow friction and heat transfer. These entropy components were used to assess the significance of viscous and heat-related flow irreversibilities and, to develop criterion of thermal optimisation for ducts. They attempted the same technique for optimising forced convection in curved ducts with longitudinal fins under laminar and turbulent conditions [17,18,19]. Whilst, the entropy approach is useful for thermal optimisation, it does not qualify as a precise technique for detecting Dean's Instability.

Fellouah et al [13,14] have developed a three-dimensional simulation model for curvature ratio $5.5 \leq \gamma \leq 20$ and aspect ratio $0.5 \leq Ar \leq 12$. With water and air as working fluids, this model was validated against their own experiments on a 180^{o} duct test section that allowed visualisation of vortex formation at different duct locations and for various Dean Numbers. They proposed the radial gradient of the axial velocity as a measure of identifying the flow instability. It is difficult to rationalise this approach because the axial velocity change in radial direction is not fundamentally connected with vortex generation. This inadequacy is clearly reflected in the work of Fellouah et al [13], where their simulation failed to detect the flow instability for some basic flow conditions observed. Chandratilleke et al [20,21] have proposed new criteria which will be re-visited for the flow situation in the current study.

Traditionally, the experimental and numerical analyses on curved ducts have been performed on rectangular duct geometries. By virtue of shape, such ducts have less wall interference on secondary vortex formation making it relatively easier for numerical modelling and convenient for experimentation including flow visualisation. Ducts with elliptical and circular cross sections have received less research attention in spite of being a common geometry used in most technological systems.

Papadopoulos and Hatzikonstantinou [22] have numerically investigated the effectiveness of internal fins in curved elliptical ducts with specific focus on friction factor and impact from fin height. Avramenko and Kuznetsov [23] have investigated Taylor-Couette and Dean flow within concentric cylindrical surface, reporting a dependency of critical Taylor and Dean numbers on the radii ratio of concave and convex walls and on the velocity slip coefficient. Simulating curved channels with elliptical cross section, Dong and Ebadian [24] and Silva et al [25] investigated the nature of flow field and vortices formed. They have observed that the stagnation regions are vastly different to those in rectangular ducts and the Dean's Instability is seen to originate within the flow rather than at the outer duct wall. Andrade et al [26] report a study with a finite element numerical model and discuss the influence from temperature dependent viscosity on heat transfer and velocity profile for fully developed forced convection in elliptical curved tube. They considered both cooling and heating cases wherein the Nusselt Number was found to be lower for variable-viscosity than with constant-properties. This was attributed to the increased viscosity at the cooler inner duct wall dampening the secondary flow and the vortex formation.

Whilst an extensive knowledge base has been established for two-phase flow in straight ducts, the flow boiling behaviour in curved fluid ducts remains very much an unexplored area although such flow geometries are commonly found as an integral part of many industrial heat transfer equipment. For reference, some notable contributions to two-phase flow in straight ducts are: Luteset [27] experimentally investigated the transition of nucleate to film boiling on a flat surface, reporting heat flux rates almost three times the critical heat flux for pool boiling; Shiotsu and Hama [28] conducted forced convection film boiling experiments in a vertical cylinder and a correlation was suggested for boiling heat transfer with thermal radiation; Liu et al [29] developed one of the most up-to-date theoretical models for predicting critical heat flux for sub-cooled flow boiling; Baduge et al [30] experimentally investigated the boiling heat transfer in vertical capillary tubes and demonstrated that in vertical capillary tubes, the slug-annular and annular flow dominated the flow patterns while the liquid film evaporation was the primary heat transfer mechanism. Forming the basis for most numerical work, the Rensselaer Polytechnic Institute (RPI) has developed a two-phase flow boiling model, where the wall heat flux is broken up into three components, namely the heat transfer through liquid, that due to quenching and liquid evaporation. The model assumes thermal equilibrium between the vapour and liquid phases.

Publications on flow boiling in curved ducts are rather limited due to the modelling complexities arising from mutually interacting two-phase and secondary flow mechanisms. In curved ducts, the centrifugal forces drive the heavier liquid component of two-phase flow towards the outer duct wall while displacing the lighter vapour phase towards the inner wall. Consequently, unsymmetrical flow patterns are generated with fundamental changes to phase formation and affecting the heat transfer characteristics.

For flow boiling in curved ducts, Sturgis and Mudawar [31] have reported essentially a single phase model where a wavy distribution was assumed for the vapour phase with liquid occupying the troughs of the wave called wetting fronts. They developed a CHF model for long curved surfaces through considerations of separated flow, thermal energy balance, interfacial instability and bubble lift-off criterion. These models were limited in scope for neglecting the interfacial condensation and were applicable only for near-saturated

boiling conditions. Jo et al [32] numerically investigated the two-phase flow heat transfer in helical tubes of pressurised water reactor steam generator using a CFX code. Both the RPI boiling model and the bulk boiling model were used for the flow boiling simulations on a vertical straight duct and helical channel. They reported the formation of a liquid film on the opposite side of helix axis, which was attributed to the centrifugal force effect in curved sections, and discussed forms of heat transfer in flow passages. Predicted results showed good agreement with experimental data.

The current study examines the boiling characteristics in curved ducts and compares them with those in straight ducts to understand the unique behaviour brought about by duct curvature. In this, a two-phase turbulent simulation model is developed using a non-equilibrium wall heat flux partitioning approach that permits the vapour phase temperature to increase beyond saturation temperature. This essentially eliminates the limiting assumption of vapour-liquid equilibrium used in the Rensselaer Polytechnic Institute (RPI) approach and represents a more realistic modelling methodology for flow boiling with high vapour volume fraction.

NOMENCLATURE

Ar	[m^2]	Aspect Ratio, a/b
A_i	[m^2]	Interfacial area
a	[mm]	Height of cross section
b	[mm]	Width of cross section
Be	[-]	Bejan Number
C_P	J/kg.K	Specific heat capacity
C_{pq}	J/kg-mol.K	Isobaric heat capacity of phase-q
D	[m]	Tube diameter
D_h	[mm]	Hydraulic diameter
d_b	[m]	Bubble diameter
$\vec{F}_{cy}$	[N]	Centrifugal force
$\vec{F}_{q-body}$	[N]	Body forces on phase-q
$\vec{F}_{lift}$	[N]	Lift force
$\vec{F}^{D}{}_{pq}$	[N]	Drift force of phase-p on phase-q
$\vec{F}^{TD}{}_{pq}$	[N]	Turbulence drift force of phase-p on phase-q
G	[kg/m^2.s]	Mass flow rate
G_k, G_ε	[-]	Turbulence kinetic energy and dissipation rate production terms
g	[m/s^2]	Gravitational acceleration
H^*	[-]	Dimensionless Helicity
h	[W/m^2.K]	Heat transfer coefficient
h_{sl}	[W/m^2.K]	Ranz-Marshal heat transfer coefficient
h_{pq}	[kJ/kg]	Inter-phase enthalpy
h_{fg}	[kJ/kg]	Latent heat of evaporation
$\Delta h_{standard}$	[J/kg-mol]	Enthalpy difference between phases
k	[m^2/s^2]	Turbulence kinetic energy
k_f	[W/m.K]	Bulk thermal conductivity
L_H	[m]	Length of heated section
L_{NH}	[m]	Length of non-heated section
$\dot{m}_{pq}$	[kg/s]	Mass transfer from phase-p to phase-q
Nu	[-]	Nusselt number
p	[MPa]	Pressure
p^*	[-]	Dimensionless static pressure
R	[m]	Duct radius of curvature
Re_b	[-]	Bubble Reynolds number
Re_∇	[-]	Bubble shear Reynolds number
$\dot{q}_L$	[W/m^2]	Liquid phase heat transfer
$\dot{q}_V$	[W/m^2]	Vapour phase heat transfer
$\dot{q}_Q$	[W/m^2]	Quenching heat flux
$\dot{q}_E$	[W/m^2]	Evaporating heat flux
$\dot{q}_w$	[W/m^2]	Wall heat flux
$\vec{S}$	[-]	Coordinate along duct cross section defining secondary flow direction
S_T'''	[W/m^3.K]	Volumetric average entropy generation rate due to heat flow
S_p'''	[W/m^3.K]	Volumetric average entropy generation rate due to friction
S_g'''	[W/m^3.K]	Total entropy generation
S_T	[-]	Energy source term
S_k, S_ε	[-]	Turbulence source term in bubbly flow regime
T_{in}	[K]	Bulk inlet temperature
T_{sat}	[K]	Saturation temperature
ΔT_{sub}	[K]	Inlet subcooling temperature $(T_{sat} - T_{in})$
U_{in}	[m/s]	Duct inlet velocity
V_r	[m/s]	Axial velocity
$\vec{v}_q$	[-]	Velocity of q-phase
$\vec{v}_{pq}$	[-]	Relative density of p-phase to q-phase
v_{xq}, v_{yq}, v_{zq}	[m/s]	Velocity components of phase-q
u^*, v^*, w^*		Dimensionless velocity components
x, y, z	[m]	Coordinates
y^+	[-]	Dimensionless wall distance

Special characters

α		Volume of fraction
ε	[m^2/s^3]	Turbulence dissipation rate
γ	[-]	Curvature ratio, b/R
μ	[kg/m.s]	Bulk viscosity
ρ	[kg/m^3]	Bulk density
τ	[-]	Viscous stress tensor
τ^T	[-]	Turbulence stress tensor
$\tau^T{}_T$	[-]	Temperature turbulence stress tensor

MODEL DESCRIPTION AND NUMERICAL ANALYSIS

Fig. 1 shows the rectangular and elliptical geometries used for the three-dimensional simulation model in the current study. It consists of a semi-circular curved duct fitted with straight inlet and outlet passages for ensuring fully developed flow at entry and smooth outflow at exit. The working fluid air having temperature dependent properties flows through the passage under steady and laminar flow conditions and is assumed to be an incompressible Newtonian fluid. The analysis focuses on the curved duct that is designated by 0^o at inlet to 180^o at outlet. Fig. 1 also shows the key geometrical parameters, duct height *a*, width *b* and the radius of curvature *R*.

Single-Phase Flow Modelling

This model solves the following governing equations:

Time-averaged continuity equation:

$$\nabla.(\vec{V}) = 0 \tag{1}$$

The momentum and energy conservation equations:

$$\vec{V}.\nabla(\rho\vec{V}) = -\nabla p + \mu\nabla^2\vec{V} + \rho_m\vec{g} + \vec{F}_c \tag{2a}$$

$$\vec{V}.\nabla(\rho c_p T) = k\nabla^2 T + S_T \tag{2b}$$

The centrifugal body force term along the radial direction is,

$$F_c = \rho\frac{V_r^2}{r} = \rho\frac{(u^2+w^2)}{\sqrt{x^2+z^2}} \tag{3}$$

Considering the position and alignment of curved geometry, centrifugal source term in system is given by,

$$\vec{F}_c = \rho\frac{1+sign(-z)}{2}\frac{(u^2+w^2)}{x^2+z^2}(x\hat{i}+z\hat{k}) \tag{4}$$

In Eq. 4, a Sign Function has been included to ensure the centrifugal source term is applied only on the curved side of the geometry (i.e. $z \le 0$). For defining dimensionless parameters, the characteristics length, velocity and pressure are chosen to be D_h, U_{in} *and* $\frac{1}{2}\rho U_{in}^2$ respectively.

For capturing the helix-like secondary fluid motion, this three-dimensional simulation model incorporates a helicity function, which is defined by Eq. 5. The helicity is non-dimensionalised using a reference helicity based on hydraulic diameter, as given in Eq. 6.

$$H = u(\frac{\partial w}{\partial y}-\frac{\partial v}{\partial z})+v(\frac{\partial u}{\partial z}-\frac{\partial w}{\partial x})+w(\frac{\partial v}{\partial x}-\frac{\partial u}{\partial y}) \tag{5}$$

$$H \approx \frac{U_{in}^2}{D_h} \Rightarrow H^* = H(\frac{D_h}{U_{in}^2}) \tag{6}$$

For identifying the inception of hydrodynamic flow instability, the model proposes two separate criteria. The first criterion is based on helicity, which is computed from Eq. 6.

The second criterion uses the outer duct wall pressure gradient profile for which the non-dimensional wall pressure gradient is obtained from Eq. 7. A sign convention is incorporated for Eq. 7 to designate the opposite rotational directions of the vortices in upper and lower half of duct cross section, following the selection of coordinate *S* along duct cross section, as depicted in Fig. 1(b).

$$\frac{dp^*}{d\vec{S}} = \begin{cases} -\dfrac{D_h}{\frac{1}{2}\rho U^2{}_{in}}\dfrac{dp}{ds} & \text{At lower half of duct} \\ \dfrac{D_h}{\frac{1}{2}\rho U^2{}_{in}}\dfrac{dp}{ds} & \text{At upper half of duct} \end{cases} \tag{7}$$

For the forced convective heat transfer in the duct, the local Nusselt Number is defined as $Nu = \frac{hD}{k}$ where the heat transfer coefficient h, is determined by considering the grid cell temperature difference between the heated wall and the adjacent fluid cell. The average Nusselt number is obtained from the surface integral, $\overline{Nu} = \frac{1}{A}\int_A NudA$.

The model uses fluid irreversibility as a technique for thermal optimisation. This approach considers the overall entropy generation to be contributed by wall heat transfer that is essentially the thermally-induced buoyancy effects and, fluid friction arising from secondary flow driven by centrifugal forces. As such, the components of entropy generation from heat transfer (S_T) and that from fluid friction (S_p) within the solution domain are computed for Eq. 8 (a), (b) and (c).

$$S_T = \frac{k}{T^2}\left[(\frac{\partial T}{\partial x})^2+(\frac{\partial T}{\partial y})^2+(\frac{\partial T}{\partial z})^2\right] \tag{8a}$$

$$S_P = \frac{\mu}{T}\Phi \tag{8b}$$

$$\Phi = 2\,[(\frac{\partial u}{\partial x})^2+(\frac{\partial v}{\partial y})^2+(\frac{\partial w}{\partial z})^2\,]+(\frac{\partial u}{\partial y}+\frac{\partial v}{\partial x})^2+(\frac{\partial w}{\partial y}+\frac{\partial v}{\partial z})^2+(\frac{\partial u}{\partial z}+\frac{\partial w}{\partial x})^2 \tag{8c}$$

The entropy terms are generalised as volumetric averaged values using,

$$S_T''' = \frac{\int S_T dv}{dv} \tag{9a}$$

$$S_p''' = \frac{\int S_p dv}{dv} \tag{9b}$$

$$S_g''' = S_T''' + S_p''' \tag{9c}$$

These volumetric entropy generation terms are combined to form Bejan number that is defined by,

$$Be = \frac{S_T'''}{S_g'''} \tag{10}$$

Bejan Number reflects the relative domination of flow irreversibility by heat flow with respect to the overall irreversibility [33]. As such, a Bejan Number of 1 indicates totally heat transfer-dominated entropy generation while 0 refers to fluid friction causing all of irreversibility. Thus for curved ducts, the Bejan number acts as a clear visual parameter that depicts the relative strength of thermally-induced buoyancy effects within the fluid stream compounded by the centrifugal forces-driven secondary flow and Dean vortices. This approach is then utilised for thermally optimising the forced convection process in ducts.

Two-Phase Flow Modelling

In flow boiling, vapour and liquid phases flow together with composition ranging from bubbly to full vapour regimes. Boiling and condensation mass transfer processes are connected to heat transfer on phase change. Among multi-phase models, the Eulerian model is reported best for it considers phases separately and solves the sets of momentum and energy equation for each phase. The volume fraction in continuity equation captures the phase boundaries wherein mass and heat transfers are also defined for each phase separately. An energy equation termed boiling closure act to as coupled correlation for heat and mass transfer in boiling/condensation processes.

This model uses the following governing equations:
The continuity equation:

$$\nabla.(\alpha_q \rho_q \vec{v}_q) = \dot{m}_{pq} - \dot{m}_{qp} \tag{11}$$

The momentum and energy conservation equations:

$$\nabla(\alpha_q \rho_q \vec{v}_q) = -\alpha_q \nabla p + \nabla.\vec{\tau}_q + \nabla.\vec{\tau}^T{}_q + \alpha_q \rho_q \vec{g} + \vec{F}^D_{pq} + \vec{F}^{TD}_{pq} + \dot{m}_{pq}\vec{v}_{pq} - \dot{m}_{qp}\vec{v}_{qp} + \vec{F}_{q-body} + \vec{F}_{lift} \tag{12a}$$

$$\nabla(\alpha_q \rho_q c_{pq} T_q) = k_{fm}\nabla^2 T_q + \nabla.\tau^T{}_{Tq} + Q_{pq} + \dot{m}_{pq}h_{pq} - \dot{m}_{qp}h_{qp} \tag{12b}$$

In Eq. 12a and 12b, $\vec{F}_{body}$ and $\vec{F}_{lift}$ are body and lift forces while $\vec{F}^D_{pq}$ and $\vec{F}^{TD}_{pq}$ are drag and turbulence drift forces, respectively. The effects of surface tension on pressure difference across phase boundaries are integrated in Eq. 12(a) by the approach suggested by Brackbill et al. [34].

Turbulence model

In flow boiling fluid is turbulent even in viscous regions. In Eq. 12(a) and 12(b), $\nabla.\vec{\tau}_q$ and $\nabla.\tau^T{}_{Tq}$ are the Reynolds stress tensor and the temperature turbulence tensor in generalised form, respectively. Depending on the model, these two terms couple the momentum and energy equations with two transport equations known as turbulent closures. Multi-phase Eulerian approach using $k-\varepsilon$ model is found to be a good compromise that is consistent with experimental results and computational needs. Hence, the $k-\varepsilon$ (RNG) turbulence model is adopted in the current simulation, as below.

$$\nabla.(\rho_m \vec{v}_m k) = \nabla^2(\mu_m + \frac{\mu_t}{\sigma_k})k + G_k - \rho_m \varepsilon + S_k \tag{13a}$$

$$\nabla.(\rho_m \vec{v}_m \varepsilon) = \nabla^2(\mu_m + \frac{\mu_t}{\sigma_\varepsilon})\varepsilon + C_{1\varepsilon}\frac{\varepsilon}{k}G_k - C_{2\varepsilon}\rho_m[\frac{\varepsilon^2}{k}] - R_\varepsilon + S_\varepsilon \tag{13b}$$

$$\mu_t = \rho_m C_\mu \frac{k^2}{\varepsilon} \tag{13c}$$

where R_ε is the additional term related to mean stress and G_k is the turbulent kinetic energy production rate. In Eq. 13, the RNG constants are,

$$\sigma_k = 1 \qquad \sigma_\varepsilon = 1.3 \qquad C_{1\varepsilon} = 1.42 \qquad C_{2\varepsilon} = 1.68 \qquad C_\mu = 0.0845 \tag{14}$$

while the bulk mixture properties are calculated from,

$$\rho_m = \sum_{i=1}^{2}\alpha_i \rho_i \tag{15a}$$

$$\vec{v}_m = \frac{\sum_{i=1}^{2}\alpha_i \rho_i \vec{v}_i}{\sum_{i=1}^{2}\alpha_i \rho_i} \tag{15b}$$

The specific turbulence source terms S_k and S_ε for turbulent bubbly regime (boiling case) in Eq. 13 are obtained from the results of Troshko and Hassan [35] as,

$$S_k = 0.75 C_{drag}(\rho_l \alpha_v / d_b)|\vec{v}_v - \vec{v}_l|^2 \tag{16a}$$

$$S_\varepsilon = 1.35 C_{drag}(S_k / d_b)|\vec{v}_v - \vec{v}_l| \tag{16b}$$

For the Eulerian model, the lift and virtual mass source terms are defined through established methods and correlations. However to obtain stable solutions, the characteristics of phase interaction require precise adjustment depending on the physical and numerical condition for boiling. These parameters to be considered are briefly explained below.

Non-Equilibrium model

The current two-phase flow simulation is developed as a non-equilibrium model and overcomes a major modelling drawback in the RPI approach, which assumes thermal equilibrium between liquid and vapour phases. Following the RPI method, the present approach evaluates three wall heat partitioning components, namely the liquid convective, quenching and evaporative heat fluxes. Making the simulation more realistic, the model also includes a fourth heat partitioning component to account for diffusive heat flux of vapour bubble phase. This eliminates the equilibrium assumption of vapour at saturation temperature used by the RPI method. The total wall heat flux is given by the summation of the four terms as,

$$\dot{q}_w = (\dot{q}_L + \dot{q}_Q + \dot{q}_E) f(\alpha_1) + (1 - f(\alpha_1))\dot{q}_V \tag{17}$$

The first three terms in Eq. 7 are the heat flux components due to liquid convection, cyclic-averaged transient heat transfer in liquid re-entering the wall region after bubble detachment and the energy for evaporative phase change. $\dot{q}_v = h_v(T_w - T_v)$ is the diffusive heat flux from wall to vapour bubble representing non-equilibrium vapour phase. The local liquid volume fraction $f(\alpha)$ is defined and given by,

$$f(\alpha) = \begin{cases} 1 - \frac{1}{2}e^{-20(\alpha_l - 0.2)} & \alpha_l > 0.2 \\ \frac{1}{2}(\frac{\alpha_l}{0.2})^4 & \alpha_l < 0.2 \end{cases} \tag{18}$$

The bubble drag force and interface heat transfer are dependent on the vapour-liquid interfacial area (A_i) which is dependent on the bubble diameter. The interfacial area is calculated from,

$$A_i = \frac{6\alpha_v(1-\alpha_v)}{D_b} \tag{19}$$

In Eq. 12(a), the Drag force $\vec{F}^D_{pq}$ for a bubbly boiling case is obtained from the correlation by Ishii and Zuber [36] as,

$$\vec{F}^D_{pq} = \frac{A_i}{8}\rho_l C_D|\vec{v}_l - \vec{v}_v| \tag{20}$$

For Eq. 20, the drag coefficient is determined by choosing the minimum of viscous regime (C_D^{vis}) and distorted regime (C_D^{dis}), which are evaluated from,

$$C_D^{vis} = \frac{24(1+0.1\,Re_b^{0.75})}{Re_b\sqrt{max(\alpha_l.0.5)}} \tag{21a}$$

$$C_D^{dis} = \frac{2d_b\sqrt{g(\rho_l-\rho_v/\sigma}}{3\times max(\alpha_l,0.5)} \tag{21b}$$

$$C_D = min(C_D^{vis},C_D^{dis}) \tag{21c}$$

In the model, the wall region is partitioned into areas covered by either bubbles or liquid. Bubble diameter of vapour phase is adjusted according to a function suggested by Kurnul and Podowski [37], as follows.

$$d_b = \begin{cases} 0.0015 & \Delta T_{Sub} < 0 \\ 0.00015 - 0.0001\Delta T_{Sat} & 0 < \Delta T_{Sub} < 13.5 \\ 0.00015 & \Delta T_{Sub} > 13.5 \end{cases} \tag{22}$$

The lift force $\vec{F}_{lift}$ in Eq. 12(a) is computed from the correlation developed by Moraga et al. [38],

$$\vec{F}_{lift} = C_{lift}\rho_l\alpha_v(\vec{v}_v-\vec{v}_l)\times(\nabla\times\vec{v}_l) \tag{23a}$$

$$C_{lift} = \begin{cases} 0.0767 & \varphi \le 6\times10^3 \\ [0.12-0.2e^{-\frac{\phi}{36000}}]e^{\frac{\phi}{3\times10^7}} & 6\times10^3 \le \varphi \le 1.9\times10^5 \\ 0.002 & \varphi \ge 1.9\times10^5 \end{cases} \tag{23b}$$

and the turbulence drift force $\vec{F}_{pq}^{TD}$ is obtained from,

$$\vec{F}_{pq}^{TD} = \rho_l k\nabla\alpha_v \tag{24}$$

where $\varphi = Re_b\,Re_\nabla$. The bubble Reynolds number and bubble shear Reynolds numbers, which are used in Eq. 23 and 24, are defined as $Re_b = d_b\rho_l|v_l-v_v|/\mu_l$ and $Re_\nabla = d_b^2\rho_l|\nabla\times\vec{v}_l|/\mu_l$, respectively.

As vapour bubbles depart the wall, the heat transfer from vapour bubble to liquid phase is given by,

$$\dot{q}_{lt} = A_i h_{sl}(T_{sat}-T_l) \tag{25}$$

where the heat transfer coefficient h_{sl} is calculated from the correlation suggested by Ranz-Marshal [39] as,

$$h_{sl} = \frac{k_l}{D_b}(2+0.6\,Re^{0.5}\,Pr^{0.33}) \tag{26}$$

Additionally, the interfacial heat transfer from liquid to vapour is given by,

$$\dot{q}_{vt} = \frac{\alpha_v\rho_v c_{pv}}{0.05}(T_{sat}-T_v) \tag{27}$$

where the time scale is taken to be 0.05. The bubble interfacial mass transfer is then calculated from,

$$\dot{m}_i = \dot{m}_{lt} + \dot{m}_{lv} = \frac{\dot{q}_{lt}+\dot{q}_{vt}}{h_{fv}} \tag{28}$$

The centrifugal body force term in Eq. 12(a) is given by,

$$\vec{F}_{q-body} = \rho_q\alpha_q\frac{(v_{xq}{}^2+v_{zq}{}^2)}{x^2+z^2}(x\hat{i}+z\hat{k}) \tag{29}$$

RESULTS AND DISCUSSION

The simulation is performed on 25 mm wide rectangular ducts with the aspect ratio varied from 1 to 6. In elliptical ducts, minor axis is fixed at 25 mm while altering the major axis to obtain aspect ratio up to 6. For all ducts, a fixed radius of curvature of 125 mm is used. A constant velocity condition is applied to the inlet of the straight duct section preceding the curved duct. The length of straight duct is chosen to achieve fully developed flow conditions at inlet of curved duct. A pressure outlet condition is applied to the final exit of the flow geometry. The air temperature is taken to be constant at 300 K at the inlet. The duct walls are assumed to have no slip boundary condition. For heated ducts, a constant heat flux is applied on the outer half of duct wall boundary.

In improving the overall computational accuracy, all fluid and thermal properties are defined as temperature dependent quantities. The buoyancy force arising from wall heating is introduced to the model by a sixth order density polynomial in terms of temperature whose coefficients obtained using published data. It was found that the linearity of the Boussinesq approximation caused some discrepancy therefore, inadequate for evaluating the wall pressure gradient. The second order upwind technique is used for discritisation of momentum and energy equation while the SIMPLE approach is used for pressure correction.

For analysis, the velocity, helicity, temperature and Bejan Number profiles were obtained at the exit plane (180˚) of elliptical curved duct for flow rates corresponding to Dean Number ranging from 80 to 1600. When Dean vortices were indicated in the flow, the simulations were re-run for that flow region with closer steps of *K* to determine the exact point of instability and the (critical) Dean number. This procedure was repeatedly applied for all aspect ratios, flow rates and heat fluxes. For thermal analysis, forced convection heat transfer from the duct wall to fluid was examined by evaluating the local and average Nusselt number at the duct wall.

For its practical significance, two-phase flow analyses were essentially performed on circular duct, with a comparison between flow boiling in curved and straight cases. These results are discussed in the following sections.

Results: Single-Phase Flow

Grid sensitivity and validation

Fig. 2 illustrates the grid dependency test conducted using the velocity derivative in y-direction at the duct outer wall. It is clear that the Schemes 4 and 5 having mesh size less than 1 mm show much better suitability than the other three schemes. The Scheme 5 is taken to be the optimum because of its slightly

larger cell volume arising from progressively varied mesh size. This approach facilitated remarkable ability in capturing the onset of vortex generation in the solution domain without causing excessive computational demand. As such, the present study performed all computations with Scheme 5 of mesh size less than 1 mm, achieving much higher accuracy than any previous reported work.

In validating results, the axial flow velocity obtained from the current model was compared with those from the two-dimensional analyses presented by Ghia and Shokhey [7], as illustrated in Fig. 3. It is seen that both magnitudes and trends of axial velocity are very favourably matched confirming the integrity of the numerical process. Fig. 3 also shows the secondary flow effect on the axial fluid velocity. It indicates a skewed peak towards the outer wall due to the centrifugal action and is characteristically different to the typical axial velocity distribution in straight ducts. This peak gradually spreads towards the centre with increasing flow rate because of the radial pressure build at the outer wall.

Fluid flow behaviour

Fig. 4 illustrates a typical growth sequence of dimensionless helicity profiles at duct exit for both rectangular and elliptical ducts with no external wall heating. It is readily noted that these patterns are fundamentally different to those in straight ducts. As shown in Fig. 4(a) even at low flow rates (or low K), the flow profile has two large counter-rotating vortices that are developed by the centrifugal action due to duct curvature.

The centrifugal body forces essentially impart two effects on the fluid flow. Firstly, it induces a positive radial fluid pressure field aimed at the outer duct wall (left wall in Fig. 4). Secondly, the centrifugal action drives the fluid towards the outer duct wall creating a lateral (or radial) fluid motion in duct cross section. This lateral fluid flow occurs adverse to the radial pressure field and is superimposed on the axial flow through the duct, thus forming the secondary flow structure that appears as counter-rotating vortices in the duct cross section.

As the axial flow is increased (larger K), the lateral fluid motion becomes stronger leading to more vigorous interaction with the outer duct wall while simultaneously intensifying the radial pressure field. In this process, the lateral fluid movement reaching the outer duct wall is slowed down by the combined action of the adverse radial pressure field and the fluid viscosity to form a stagnant flow region near the duct wall. Above a certain value of K, the radial pressure gradient becomes sufficiently strong to stop and reverse the lateral fluid flow, thus creating a weak local flow recirculation that appears to be an additional pair of vortices in the vicinity of the outer wall. This flow situation is referred to as the Dean Hydrodynamic Instability while the vortices are termed Dean Vortices. Fig. 4 (b) and Fig. 4 (c) show the typical helicity contours at the onset of hydrodynamic instability for rectangular and elliptical ducts, respectively. After inception, Dean vortices continue to grow bigger with increasing K while imparting stronger influence on the main secondary vortices and displacing them away from the duct centreline, as illustrated in Figs. 4 (b) to (e).

It is noticed that, in rectangular ducts, the Dean instability tends to occur at a lower flow rate (or K) than in elliptical ducts of the same aspect ratio. This is because, in rectangular ducts, the secondary vortex motion is less constrained by the cross sectional geometry than in elliptical ducts allowing more degree of freedom for Dean vortex generation.

Hydrodynamic instability and Dean vortices

In curved ducts, the appearance of Dean vortices is traditionally identified through tedious flow visualisation or by numerical trial-and-error approach. In the latter, simulations are repeatedly performed gradually narrowing down the range of K to obtain the critical Dean number and the flow patterns within chosen tolerance limits. This involves guesswork and significant computational time. Chandratilleke et.al [11] successfully used a criterion based on zero-potential stream function contours to identify the locations of Dean vortex generation. This approach was adequate for two-dimensional simulations, but is not useful for three-dimensional flows. The work of Fellouah et al [13] used the radial gradient of the axial velocity as a measure of identifying the flow instability. Such technique is not justifiable because the axial velocity change in radial direction is not fundamentally connected to secondary vortex generation. This inadequacy is clearly reflected in the work of Fellouah et al [13], where their simulation failed to detect Dean vortices for some basic flow conditions. For example around K = 100, Dean vortices are well observed in the current study, yet Fellouah et al and Silva et al [25] did not identify this occurrence.

As of now, a reliable technique for detecting Dean vortices is not available in literature, particularly for three-dimensional numerical simulations. Formulation of a generalised approach is considered difficult because the duct geometry strongly affects the onset of Dean vortices along with other parameters. In view of this, the current work proposes a novel approach that can be universally applied all duct shapes.

In detecting the onset of hydrodynamic instability or Dean vortices, the present model considers helicity H^* as the parameter to observe and demonstrates its suitability. The technique assigns a numerical threshold for H* and identifies the corresponding vortex contour that appears with this magnitude as Dean vortices. Through exhaustive simulation runs involving very small K increments, the current study has recognised $H^* = \pm 0.01$ to be an excellent choice for the helicity threshold in detecting the onset of Dean vortices in all cases of ducts examined. This threshold essentially depends on the accuracy required similar to defining limits for the boundary layer thickness in traditional fluid flows. The key advantage of this technique is that it can be implemented within the computational process itself rather than as a cumbersome post-simulation method, saving time with high accuracy.

Fig. 5 shows the helicity contours just before and just after the first detectable appearance of the Dean vortices (indicated by arrows) using $H^* = 0.01$. It is clearly evident that, this helicity-based technique is able to differentiate the appearance of Dean vortices within a very narrow range of K-for rectangular duct within K = 95 to 102 while for the elliptical duct within K = 230 to 235. Previous methods never provided such accuracy or ability for vortex detection signifying that this method is far superior to any reported approach including that

by Ghia and Shokhey [7] and Fellouah et al [13] using the axial velocity gradient.

Fig. 6 demonstrates the effect of duct aspect ratio on the hydrodynamic instability or critical Dean Number in rectangular and elliptical ducts, obtained from the helicity threshold method. For comparison, the figure also provides the critical Dean number from the results of Chen et al [6] for rectangular ducts. It is noted that the critical Dean number initially increases with the aspect ratio up to a certain value and then falls away for higher *K*. This trend conforms to the previously reported experimental and numerical observations. It is noted that the current model for rectangular ducts under-predicts the hydrodynamic instability compared to the experimental results of [6,7]. This is because the helicity approach can identify the onset hydrodynamic instability much early in the growth process of Dean vortices, whereas for visual detection in experiments, the vortices require to be developed to an observable size that corresponds to higher K, as illustrated with the results of Chen et al [7].

Thermal characteristics

For two selected values of K, Fig. 7 shows the helicity contours in rectangular and elliptical ducts with external heating applied to the outer duct wall on along with the corresponding fluid temperature fields. Comparing Figs. 7(a) and 4(a), it is observed that the outer wall heating sets up convective fluid circulation, which is driven by the buoyancy forces arising from thermally induced density changes. At low flow rate (low K), this fluid circulation dominates the flow characteristics while suppressing the secondary vortices. In the elliptical duct, the fluid circulation is more confined than in the rectangular duct because of the cross sectional geometry. Hence, steeper velocity and temperature gradients are developed at the outer wall for the elliptical duct compared to rectangular duct. Consequently, at low flow rate, the elliptical duct exhibits higher forced convection than the rectangular duct, as reflected by Fig. 8.

When the flow rate is increased, supported by stronger centrifugal action, the secondary vortices suppress the buoyancy-driven convection and dominate the flow characteristics. As shown in Fig. 7(b), the flow within the rectangular duct develops steeper velocity and temperature gradients in the vicinity of the outer wall. This leads to higher forced convection for rectangular ducts compared to the elliptical duct, as illustrated in Fig. 8.

Comparing helicity contours in Figs. 7(b) and 4(e), it is also noted that the outer wall heating impedes the secondary flow instability or inception of Dean vortices in both types of ducts. This is because the buoyancy-driven convection continually displaces the fluid layer at the outer wall and prevents the formation of stagnant fluid region in that vicinity, where the hydrodynamic instability would occur. Hence, the flow reversal leading to Dean vortices is not achieved. Higher wall heat fluxes adversely affect the flow conditions that trigger hydrodynamic instability and further reduce the potential for Dean vortex formation. In Fig. 9, this is clearly evident as a gradual decline in Nusselt number for both types of ducts with increased outer wall heat flux.

Thermal optimisation

Fig. 10 shows the Bejan number (Be) distribution over the curved duct cross sections. It is noted that for both rectangular and elliptical ducts at lower *K* or flow rate, thermal irreversibility dominates the flow (Be≈1 with red cast) over the entire flow cross section. As K increases, Be contours in Fig. 10 gradually shift to magnitudes less than 1 (blue cast). This indicates the favourable fluid mixing due to secondary flow transporting the hot fluid away from the heated wall to improve forced convection rates. Magnitudes of Be < 1 also signifies an increased contribution to total irreversibility from viscous effects, which would negate the overall application benefits. It is noted that rectangular ducts are less adversely affected compared to elliptical ducts by these opposing trends, which can be deployed to thermally optimise the flow through curved heated ducts.

Fig. 11 illustrates the variation of flow irreversibility components S_T, S_p and S_g with *K* for rectangular and elliptical ducts. For increased *K*, S_T steadily falls while S_p rapidly grows, during which the overall irreversibility S_g shows a minimum. This point of inflection is identified as practically the best possible "trade-off" between the highest achievable thermal benefit with least viscous penalty for curved duct flows. It is noted that the magnitude of the lowest overall irreversibility is higher for elliptical ducts than for rectangular ducts, indicating rectangular ducts would thermally better perform.

Results: Two-Phase Flow

Fluid flow and thermal behaviour

Predicted distribution of liquid and vapour phases at several cross sections are given in Fig. 12 for straight and curved ducts. This qualitative phase mapping clearly illustrates the underlying effects of secondary flow due to duct curvature.

In straight duct, the void fraction contours assume a ring profile that gradually grows along the duct length. In curved duct, the void fraction pattern depicts a marked deviation from the "axi-symmetry" observed for straight ducts. It is seen that the duct flow curvature causes the vapour phase is to be highly concentrated closer to the inner wall (left of diagram) while the liquid phase is displaced towards the outer duct wall (right of diagram). This is because, the curvature-induced centrifugal forces impart more inertia effect on the heavier liquid component, pushing it outwards. Consequently, the void fraction distribution is radially uneven over the duct cross section unlike in straight ducts. This creates favourable implications for the two-phase boiling heat transfer process, as explained below.

In straight duct, radially even vapour distribution acts as a uniform thermal barrier for wall heat flow into the liquid. In curved duct, the void fraction profile, which is biased towards the inner wall, improves heat transfer process in two ways. Firstly, it makes the liquid component to have a higher circumferential contact with the heated wall, thus increasing the potential for liquid evaporation. Secondly, at duct wall areas with thinner vapour distribution, thermal resistance to heat flow from the wall to liquid is reduced. Combination of these mechanisms results in improved overall flow boiling heat

transfer rate. This intrinsic thermal advantage in curved ducts is clearly illustrated through Fig. 13 and 14.

Fig. 13 provides the axial variation of the cross sectional void fraction (radially-averaged) for both curved and straight ducts at two liquid subcooling values. Considering void fraction for a given axial location, it is observed that flow boiling in curved duct produces higher volume of vapour than the corresponding straight duct, regardless of liquid subcooling. Also it is noted that, flow boiling in a curved duct requires shorter length to generate certain void fraction in the flow than in a straight duct. Thus, it is clearly evident that the duct curvature acts as a catalyst for enhancing flow boiling effectiveness. Fig. 14 provides further support for this thermal improvement.

In Fig. 14, the axial variation of radially-averaged wall superheat is presented for two liquid subcooling values for both curved and straight ducts. In straight duct, the wall superheat rapidly increases from duct inlet and then gently falls off as the vapour generation or flow boiling builds up. To the contrary in a curved duct, the axial wall superheat remains virtually constant at a much reduced value (about 12 times less) over the entire heated duct. This behaviour implies that the flow boiling in curved duct begins much closer to the duct inlet than in straight duct and the duct curvature makes the vapour generation process more efficient. Also, it is observed that a curved duct produces the flow with a given void fraction over a shorter heated length than the corresponding straight duct, highlighting the improved boiling efficiency.

Flow boiling thermal enhancement in curved duct is attributed to the skewed profile of void fraction typically illustrated in Fig. 12. This vapour distribution concentrated around the inner duct wall allows the liquid component to have a higher contact area with the heated wall whereby the potential for liquid evaporation is increased and the wall superheat is reduced. As such, curved ducts show reduced susceptibility to duct wall burnout. It is also deduced from Fig. 14 that the flow boiling process in curved duct is much less sensitivity to liquid subcooling than that in straight duct. These trends provide conclusive vindication of the very unique thermal benefits realisable in flow boiling within curved ducts.

Wall heat flow mechanisms

A pivotal aspect of the current simulation based on non-equilibrium model is to appraise the wall heat flux components contributing to the overall heat flow. In this, the components considered are: (a) evaporation heat flow (b) heat transfer due to wall quenching (c) diffusive heat in single phase liquid and (d) diffusive heat in single phase vapour. Fig. 15 illustrates the characteristics of these components along the heated duct, where Fig. 15(a) shows the duct geometry, Fig. 15(b) depicts the profiles for straight duct and, Figs. 15(c), (d) and (e) respectively indicate the profiles for curved duct at planes AA (*inner wall*), BB (*side wall*) and CC (*outer wall*).

With reference to Fig. 15(b) depicting the straight duct heat flux behaviour, it is seen that, up to about x/W = 0.3, the wall heat flow is dominated by the evaporative component while the diffusive heat flow into vapour gradually becomes stronger due to the increased vapour production. Both liquid phase and quenching heat transfer components remain relatively small and insignificant. The two-phase boiling process practically limited up to around x/W = 0.3, where the departure from nucleate boiling (DNB) occurs with the diminishing liquid evaporation leading to duct wall dry-out. Then the wall heat flux is essentially becomes single phase heat flow in to dry vapour with large duct wall superheat.

Curved duct's unique thermal behaviour in flow boiling is well revealed by the heat flux profiles at AA, BB and CC. The profile for AA in Fig. 15(c) is much similar to the straight duct behaviour in Fig. 15(b) and is dominated by the vapour diffusive heat flow. The evaporative, liquid phase and quenching heat flux components are insignificantly small and confined to very short length following duct inlet. This implies that the inner duct wall very quickly reaches dry-out conditions, which is to be expected as the curvature effect readily displaces the generated vapour towards the inner duct wall. The overall heat flux along AA remains predominantly single phase vapour heat flow with large wall heat superheats and duct wall dry-out. The profiles along BB and CC given in Fig. 15(d) and (e) portray much similar characteristics. In these, the single phase vapour heat flow component is almost non-existent over the entire duct length indicating that the heated wall is primarily exposed to liquid phase. Along the duct length, the flow boiling occurs without DNB or dry-out. These are attributed to the heavier liquid phase being driven towards the outer duct wall by the curvature-induced centrifugal forces, as typically demonstrated in Fig. 12.

Having a large liquid fraction in contact with the outer duct wall significantly increases the evaporative wall heat flux component compared to the cases of Fig. 15(b) (straight duct) and Fig. 15(c) (curved duct inner wall). The heat flow contributions from single liquid phase and quenching are also significant unlike in straight duct or along AA for curved duct. These elevated heat flows combine to provide much higher overall wall heat flux for curved duct than flow boiling in identical straight duct.

From the above comparative analysis with straight duct, it is recognised that the curved duct geometry brings about secondary flow fluid interaction to the flow boiling process that will delay the departure from nucleate boiling and dry-out at the wall while enhancing the wall heat transfer and reducing the wall superheat. In view of dry-out and burn-out issues in boilers tubes, the identified thermal benefits of flow boiling within curved duct geometry are practically significant and meaningful for sustainable energy resource usage.

CONCLUSIONS

This paper provided a broad overview of the reported numerical and experimental studies on both single and two phase fluid flows in curved flow geometries. It then presented the details of an extensive research programme that developed new methodologies for clearer fundamental understanding on fluid and thermal behaviour in curved ducts.

Improving modelling accuracy over published methods, the current study formulated a novel three-dimensional simulation methodology based on helicity for realistic representation of secondary vortex structures. The model accurately identified

and predicted the unique features of secondary flow and the associated forced convection heat transfer in rectangular and elliptical curved ducts. Conforming to the limited data in literature, the predicted results examined the effects of fluid flow rate, duct aspect ratio and heat flux over a wide practical range. The duct geometry and aspect ratio critically influenced the secondary flow characteristics with a profound effect on Dean vortex formation, Dean Instability and forced convection. Elliptical ducts showed inferior thermal performance compared to rectangular ducts under similar operating conditions.

To overcome current limitations, the study proposed two novel techniques for identifying the onset of Dean Instability in curved ducts, where one approach used a defined helicity threshold and the other considered the changes to outer wall pressure gradient. Both methods could be integrated into and performed through a computational scheme for fast, reliable and accurate detection of Dean vortex formation. However, the helicity threshold method was more universally applied to all duct shapes and aspect ratios while the pressure gradient approach showed limited functionality for over-predicting critical Dean Number.

The study demonstrated a useful technique for duct thermal optimisation based on the Second Law irreversibilities. It identified the elliptical ducts to have less favourable overall thermal characteristics than rectangular ducts.

Extending the analytical research to complex multi-phase flow, the study also successfully developed a numerical simulation for two-phase flow boiling in curved duct. This was formulated by incorporating a non-equilibrium model with wall heat partitioning, Eulerian multi-phase approach and k-ε turbulence modelling. The model produced consistent and stable results that were validated against experimental values with a good agreement. The simulation identified the unique features of flow boiling within curved ducts, where the secondary flow arising from curvature-induced centrifugal effects significantly altered the boiling regimes and heat transfer characteristics compared to straight ducts.

This numerical analysis concluded that the secondary flow interaction from duct curvature had the intrinsic ability to enhance the thermal effectiveness of flow boiling process by increasing the wall heat flux rates, reducing the wall superheat, delaying the departure from nucleate boiling (DNB) and significantly lowering the wall dry-out possibilities. Compared to straight ducts, the flow boiling in curved ducts could produce vapour at a higher rate with a shorter duct length and without much sensitivity to liquid subcooling.

REFERENCES

[1] Dean, W.R., Fluid motion in a curved channel, Proc. Roy. Soc. London Ser, A 121 (1928) 402–420.

[2] Moffatt, H.K., Viscous and resistive eddies near a sharp corner, Journal of Fluid Mechanics, 48 (1) (1964) 1–18.

[3] Eustice, J., Experiments of streamline motion in curved pipes, Proc. Roy. Soc. London Se, 85 (1).

[4] Baylis, J.A., Experiments on laminar flow in curved channels of square section, Journal of Fluid Mechanics. 48 (3) (1971) 417–422.

[5] Humphrey, J.A.C., Taylor, A.M.K., Whitelaw, J.H., Laminar flow in a square duct of strong curvature, Journal of Fluid Mechanics, 83 (1977) 509–527.

[6] Cheng, K.C., Nakayama, J., Akiyama, M., Effect of finite and infinite aspect ratios on flow patterns in curved rectangular channels, in: Flow Visualization International Symposium, Tokyo, (1977) p. 181.

[7] Ghia, K.N., Sokhey, J.S., Laminar incompressible viscous flow in curved ducts of rectangular cross-section, Trans. ASME I: Journal of Fluids Engineering, 99 (1977) 640–648.

[8] Sugiyama, Hayashi, Taro, Yamazaki, Koji, Flow Characteristics in the Curved Rectangular Channels, Bullletin of JSME, 26 (216) (1983), 532-552.

[9] Chandratilleke, T.T., Secondary flow characteristics and convective heat transfer in a curved rectangular duct with external heating, 5th World Conference On Experimental Heat Transfer, Fluid Mechanics and Thermodynamics, Thessaloniki, Greece, September 2001.

[10] Chandratilleke, T.T., Performance enhancement of a heat exchanger using secondary flow effects, in: Proc. of 2nd Pacific—Asia Conf.Mech. Eng., Manila, Philippines, September 1998.

[11] Chandratilleke, Tilak T., Nursubyakto. "Numerical prediction of secondary flow and convective heat transfer in externally heated curved rectangular ducts." International Journal of Thermal sciences 42 (2002). 187–198.

[12] Yanase, S. R. N. M., Kaga, Y. "Numerical study of non-isothermal flow with convective heat transfer in a curved rectangular duct." International Journal of Thermal Sciences 44 (2005), 1047–1060.

[13] Fellouah, H., Moctar, A. Ould El, Peerhossaini, H., "A criterion for detection of the onset of Dean instability in Newtonian fluids." European Journal of Mechanics B/Fluids 25 (2006), 505–531.

[14] Fellouah, H., Castelain, Ould-El-Moctar, Peerhossaini, H., The Dean instability in power-law and Bingham fluids in a curved rectangular duct, Journal of Non-Newtonian Fluid Mech. 165 (2010) 163–173.

[15] Guo, Jiangfeng, Xu, Mingtian, Cheng, Lin, Second law analysis of curved rectangular channels, International Journal of Thermal Sciences 50 (2011) 760-768.

[16] Ko. T.H, Ting, K., Entropy generation and optimal analysis for laminar forced convection in curved rectangular ducts: A numerical study, International Journal of Thermal Sciences 45: (2006) 138–150.

[17] Ko. T. H. "Numerical investigation on laminar forced convection and entropy generation in a curved rectangular duct with longitudinal ribs mounted on heated wall." International Journal of Thermal Sciences 45 (2005), 390–404.

[18] Ko. T. H. "A numerical study on entropy generation and optimization for laminar forced convection in a rectangular curved duct with longitudinal ribs." International Journal of Thermal Sciences 45 (2006), 1113–1125.
[19] Ko. T.H, C.P. Wu, A numerical study on entropy generation induced by turbulent forced convection in curved rectangular ducts with various aspect ratios." International Communications in Heat and Mass Transfer. 36(2008) 25-31.
[20] Chandratilleke, Tilak T, Nadim, Nima and Narayanaswamy, Ramesh, Secondary flow characteristics and prediction of Dean vortices in fluid flow through a curved duct, 6th Australasian Congress on Applied Mechanics, Perth, Western Australia, Australia, December 12th-15th 2010.
[21] Chandratilleke, Tilak T, Nadim, Nima and Narayanaswamy, Ramesh, Entropy-based secondary flow characterisation and thermal optimisation of fluid flow through curved heated rectangular ducts, 9th Astralasian Heat and Mass Transfer Cconference – 9AHMTC, Melbourne, Victoria, Australia, November 2nd-4th, 2011.
[22] Papadopoulos, P.K., Hatzikonstantinou, P.M., Numerical study of laminar fluid flow in a curved elliptic duct with internal fins, International Journal of Heat and Fluid Flow 29 (2008) 540–544.
[23] Avramenko, A.A., Kuznetsov, A.V., Instability of a slip flow in a curved channel formed by two concentric cylindrical surfaces, European Journal of Mechanics B/Fluids 28 (2009) 722–727.
[24] Dong Z.F., Ebadian M.A., Numerical analysis of laminar flow in curved elliptic ducts, J. Fluid Eng. 113 (1991) 555-562.
[25] Silva, Ricardo Junqueira, Valle, Ramon Molina, Ziviani, Marcio, Numerical hydrodynamic and thermal analysis of laminar flow in curved elliptic and rectangular ducts, International Journal of Thermal Sciences (1999) 38, 585-594
[26] Andrade, Claudia R. and Zaparoli, Edson L., Effect of temperature-dependent viscosity on fully developed laminar forced convection in curved duct, International communication in heat and mass transfer, vol.28(2), (2001) pp211-220.
[27] Lutset, M. O., Experimental Study of Temperature Distribution in the Vicinity of Film Boiling. Heat and mass transfer and physical gas dynamics, Vol.38 (2000), No. 4, pp. 623-630.
[28] Shiotsu, M., Hama, K., Film boiling heat transfer from a vertical cylinder in forced flow of liquids under saturated and sub-cooled conditions at pressures. Nuclear Engineering and Design Vol.200 (2000), pp.23–38.
[29] Liu, W., Nariaib, H., Inasaka, F., Prediction of critical heat flux for sub-cooled flow boiling. International Journal of Heat and Mass Transfer. Vol.43(2000), pp.3371-3390.
[30] Baduge, Sumith, Kaminaga, Fumito, Matsumura, Kunihito, Saturated flow boiling of water in a vertical small diameter tube, Experimental Thermal and Fluid Science. Vol.27 (2003), pp.789–801.
[31] Sturgis, J. Christopher, Mudawar, Issam, Critical heat flux in a long, curved channel subjected to concave heating, International Journal of Heat and Mass Transfer Vol.42 (1999), pp.3831-3848.
[32] Jo, Jong Chull, Kim, Woong Sik, Choi, Chang-Yong, Lee, Yong Kab, Numerical Simulation of Subcooled Flow Boiling Heat Transfer in Helical Tubes, ASME Journal of Pressure Vessel Technology, Vol.131 (2009), 011305-1.
[33] Bejan, Adrian, Entropy Generation Optimization, (1996), CRC Press Inc.
[34] Brackbill, J.U., Kothe, D.B., Zemach, C., A continuum method for modelling surface tension, Journal of computational Physics, Vol. 100 (1992), pp. 335-354.
[35] Troshko, A.A., Hassan, Y.A., A two-equation turbulence model of turbulent bubbly flows, International Journal of Multi-phase Flow Vol.27 .(2001), pp.1965-2000.
[36] Ishii, M., Zuber, N., Drag Coefficient and Relative Velocity in Bubbly, Droplet or Particulate Flows, AlChE Journal, Vol.25(1979), No.5, pp.843-855.
[37] Kurul, N. and Podowski, M.Z., On the modelling of multidimensional effects in boiling channels. Proceedings of the 27th national heat transfer conference, (1991), Minneapolis, Minnesota, USA.
[38] Moraga, F.J., Bonetto, R.T., Lahey, R.T., Lateral force on spheres in turbulent uniform shear flow. International journal of Multiphase flow. Vol. 25(1999), 1321-1372.
[39] Ranz, W.E. and Marshal, W.R., Evaporation from dros, Part i and Part ii. Chm. Eng. Prog. Vol. 48(4) (1952), 173-180.

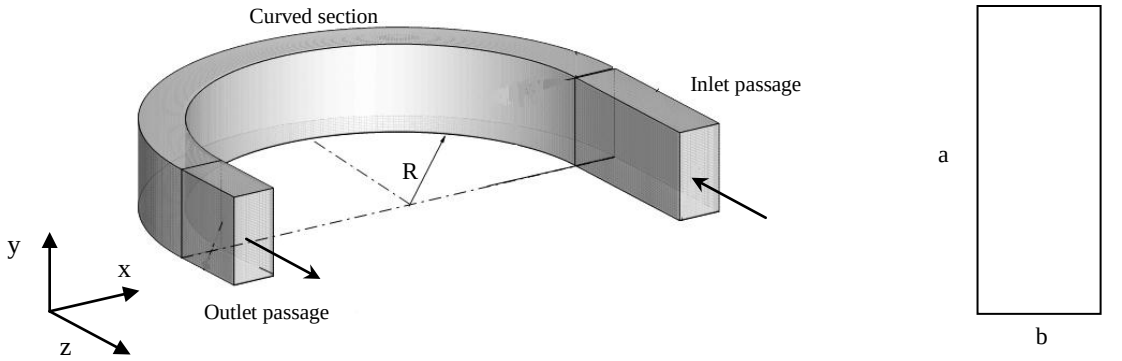

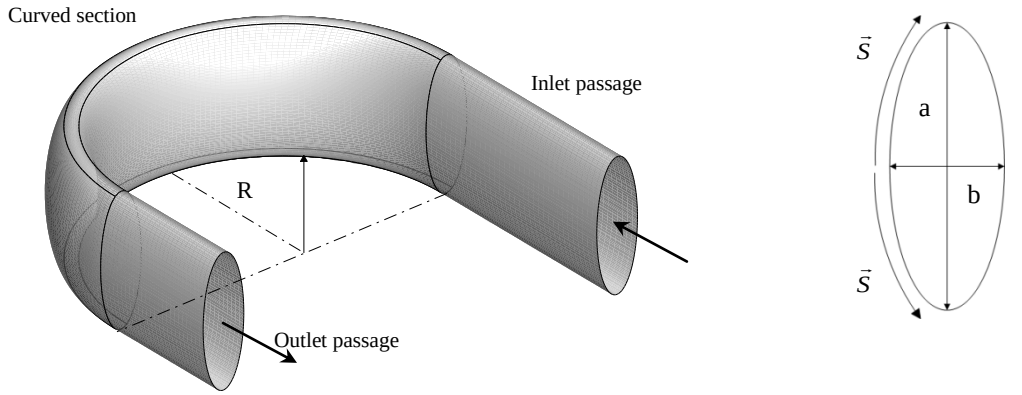

Fig.1 Computational geometry for curved duct model

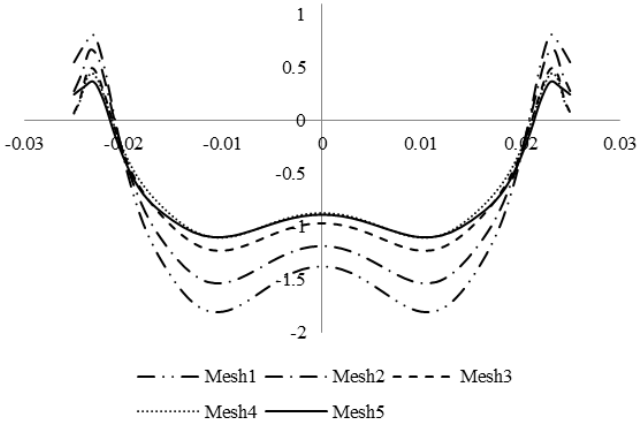

Fig. 2 Grid independancy using velocity derivative in y-direction at rectangular duct exit (K=130, Ar = 2)

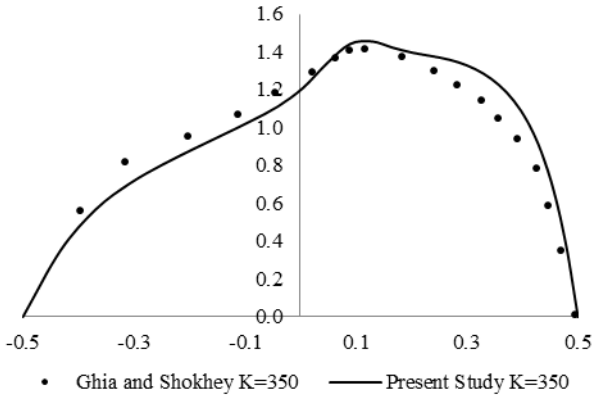

Fig. 3 Comparison of dimensionless axial velocity profile at middle plane (y = 0) along x-axis (Ar = 1)

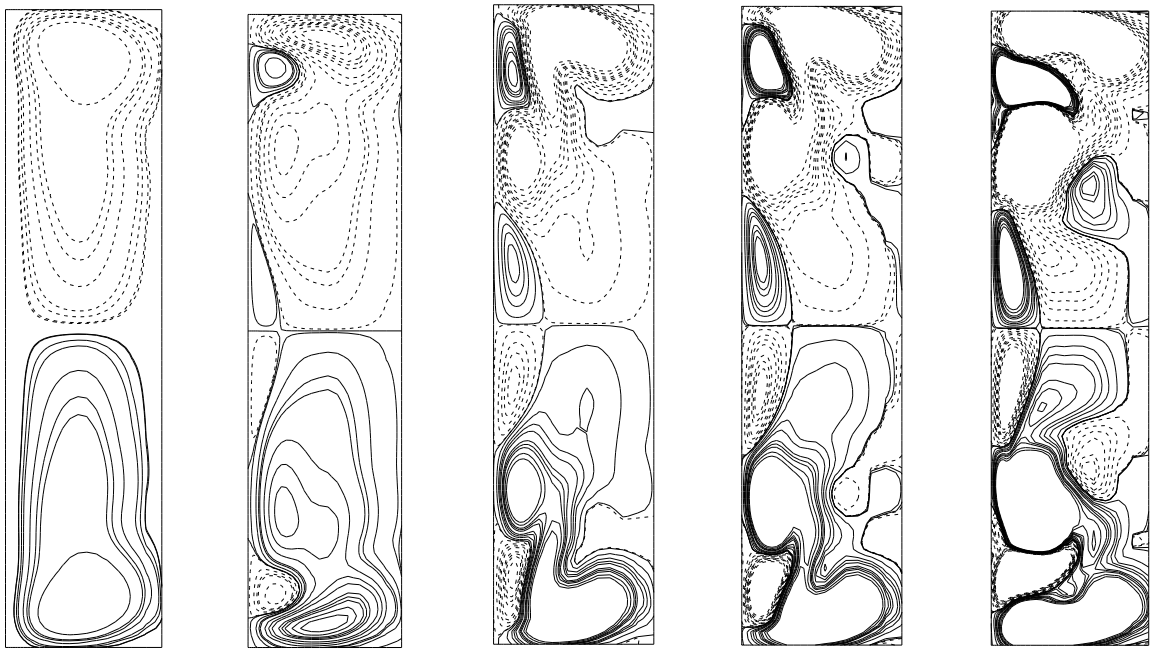

(a) K=80 (b) K=180 (c) K=260 (d) K=300 (e) K=380

Rectangular duct

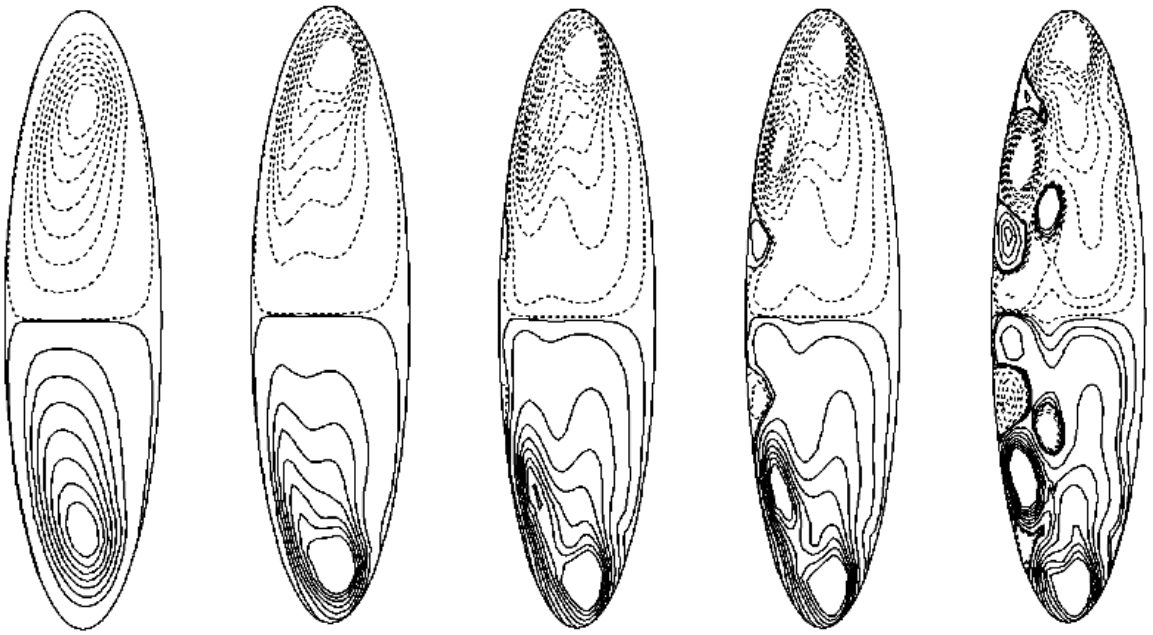

(a) K=80 (b) K=180 (c) K=260 (d) K=300 (e) K=380

Elliptical duct

Fig. 4 Dimensionless helicity contours in rectangular and elliptical ducts for varied flow rates with no wall heating (Ar = 4)

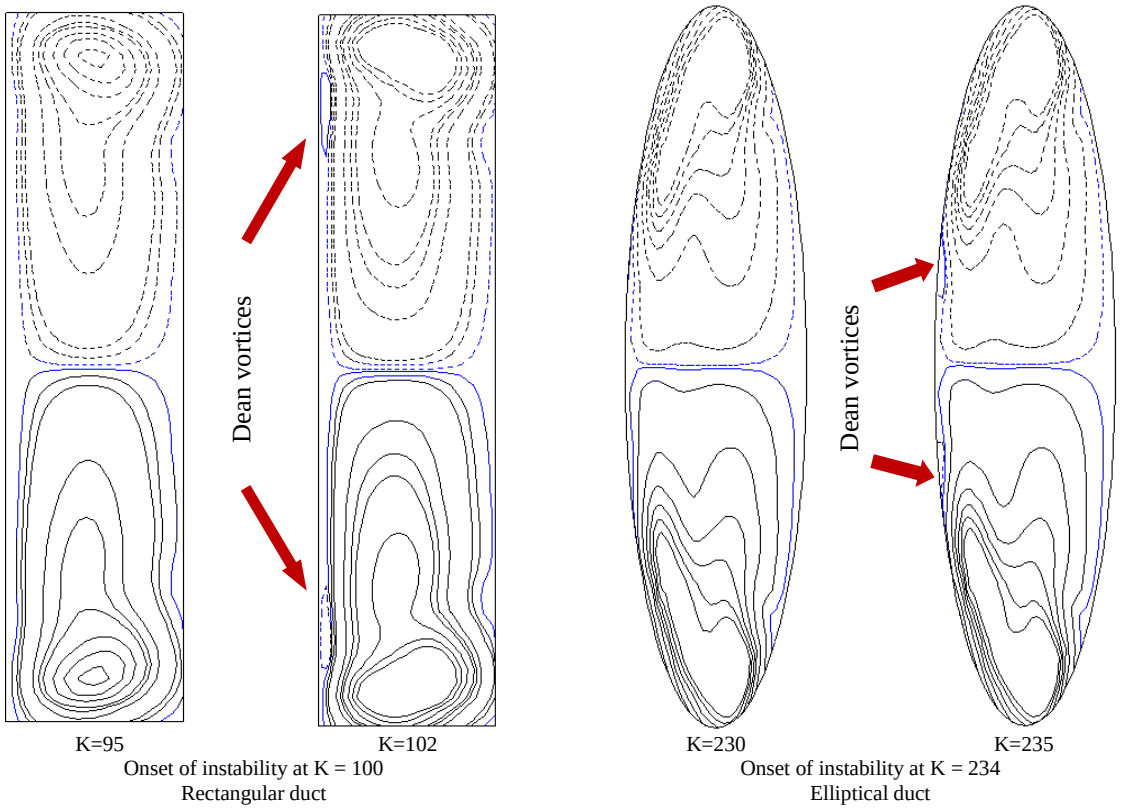

Fig. 5 Detection of the onset of Dean vortices using helicity method and threshold H* = ± 0.01 (Ar = 4, γ = 5)

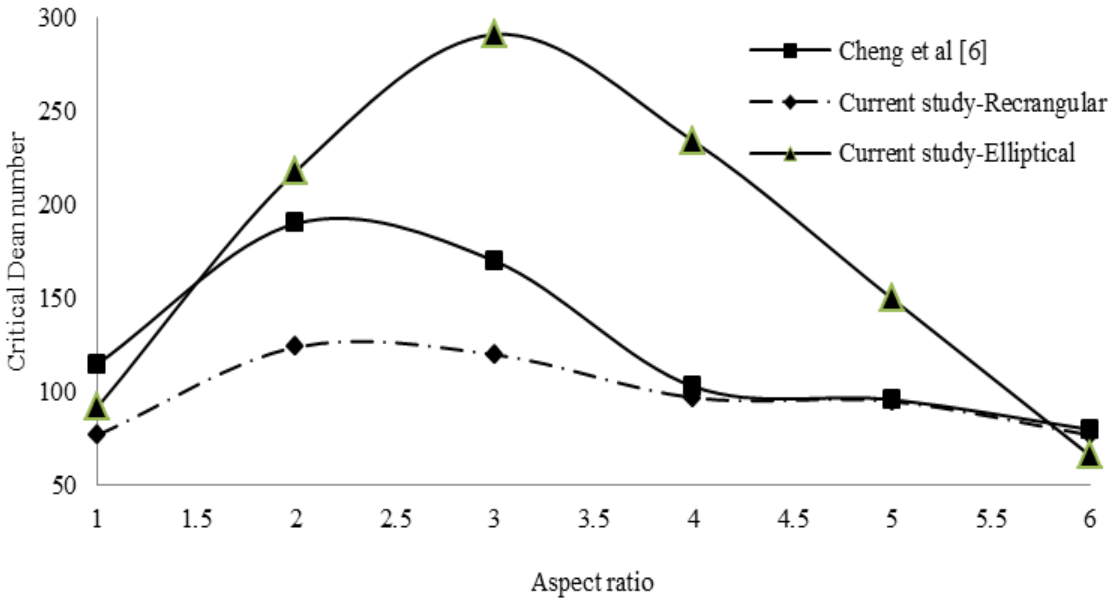

Fig. 6 Effect of aspect ratio on critical Dean number at onset of hydrodynamic instability (γ = 5)

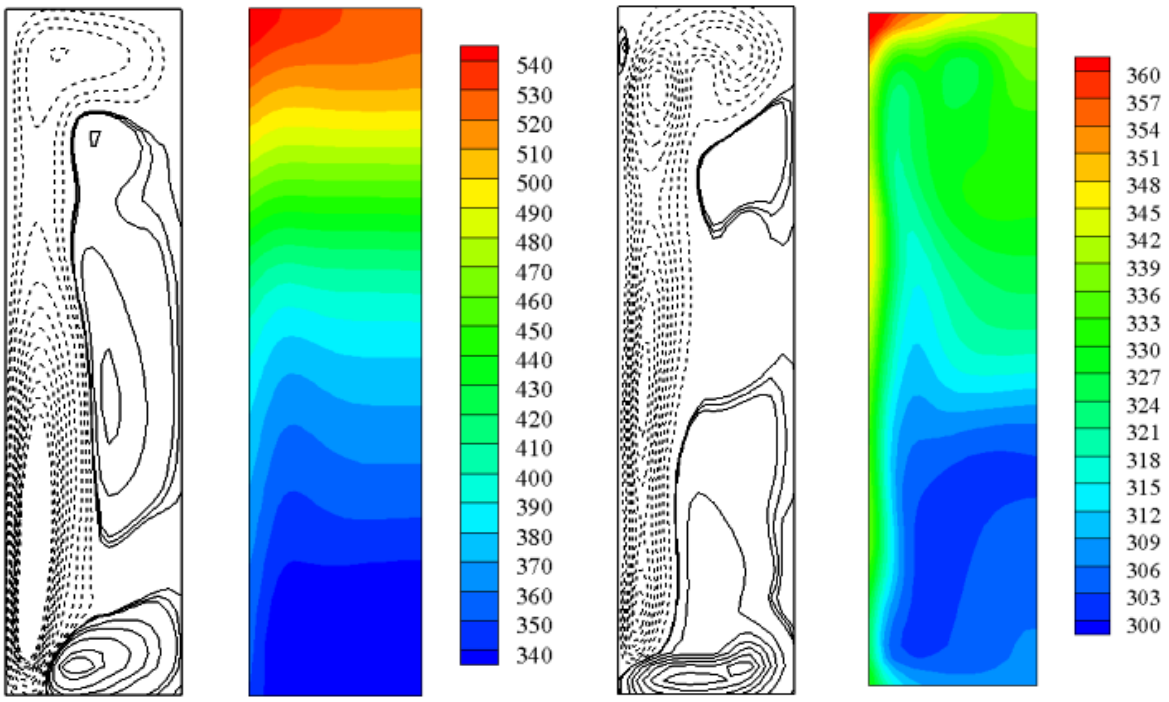

Helicity profile | Temperature field | Helicity profile | Temperature field

(a) K=80 (b) K=380

Rectangular duct

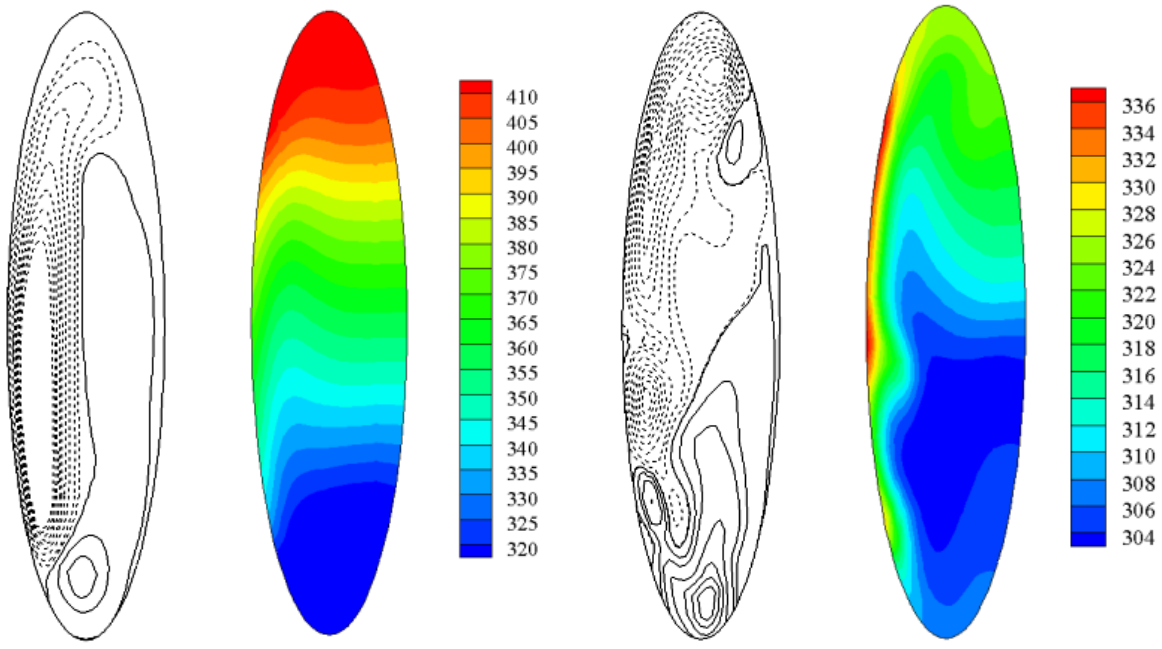

Helicity profile | Temperature field | Helicity profile | Temperature field

(a) K=80 (b) K=380

Elliptical duct

Fig. 7 Outer wall heating effect on helicity and temperature (q = 250 W/m^2, Ar = 4)

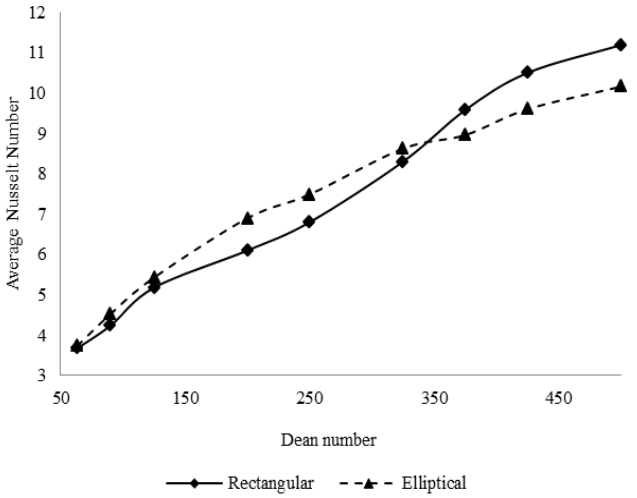

Fig. 8 Variation of average Nusselt number at outer wall with Dean number (Ar = 4, q = 250 W/m^2)

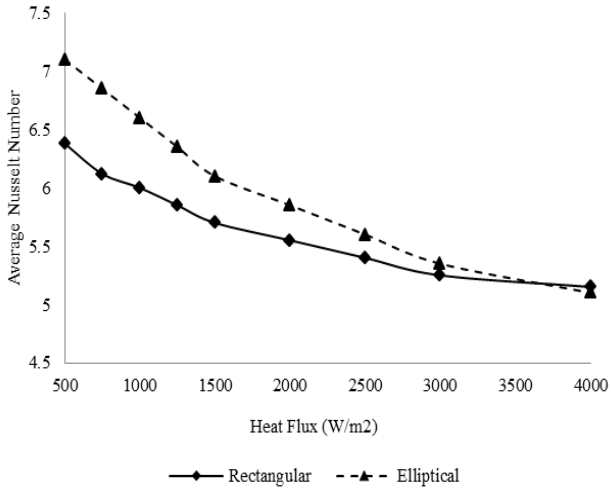

Fig. 9 Variation of average Nusselt number at outer wall with wall heat flux (Ar = 4, K=250)

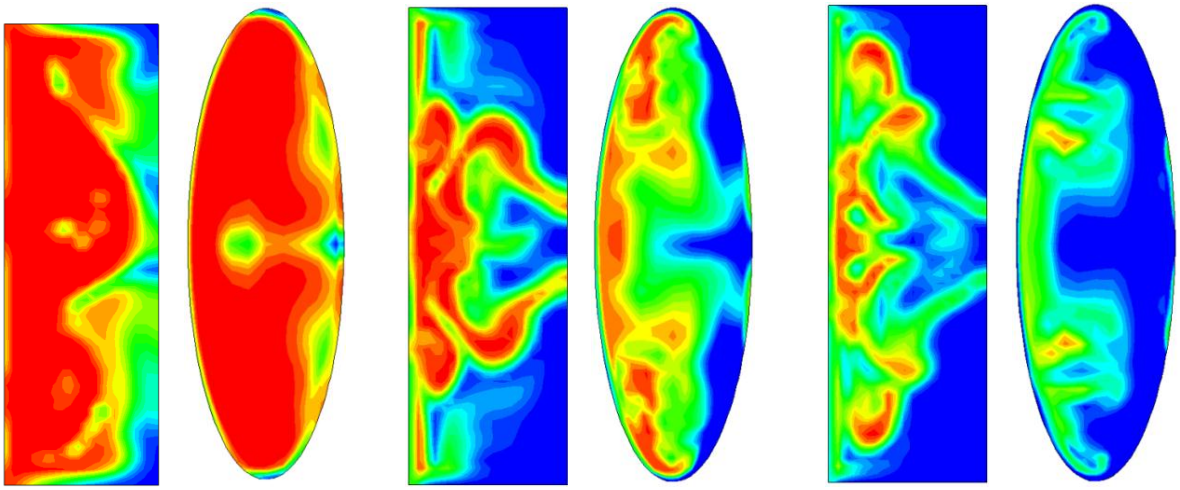

K = 400 K = 1000 K = 1600,

Fig. 10 Bejan Number contours for rectangular and elliptical curved ducts at exit (180^o) (q = 100 W/m^2)

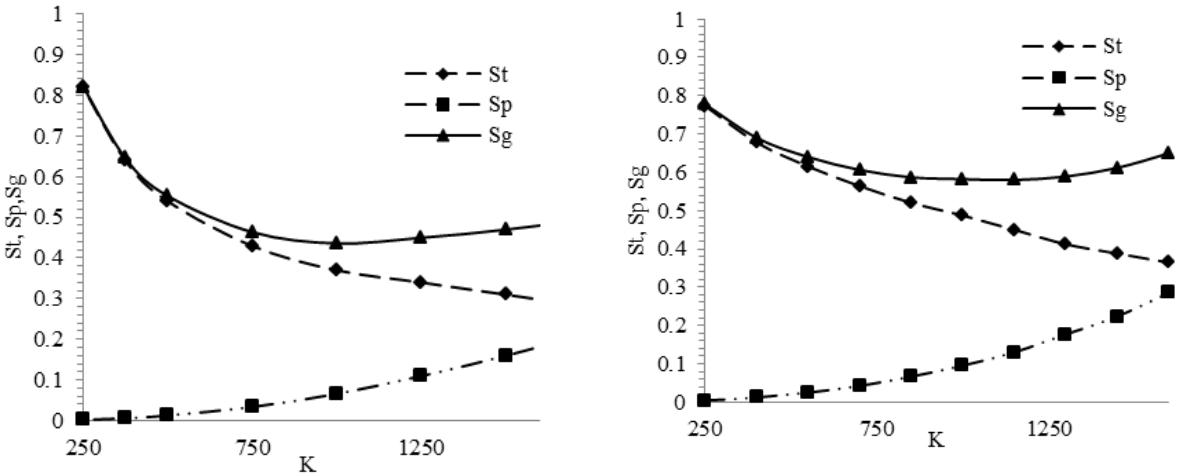

Rectangular duct Elliptical duct

Fig. 11 Curved duct thermal optimisation using total entropy generation

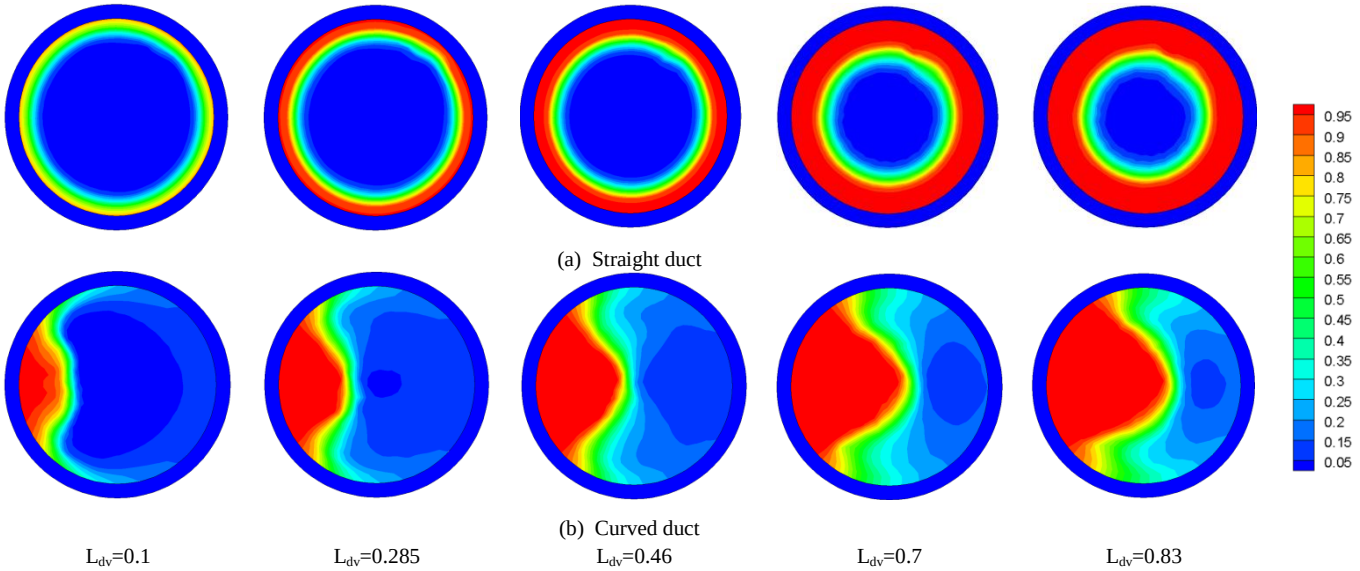

(a) Straight duct

(b) Curved duct

L_{dv}=0.1 L_{dv}=0.285 L_{dv}=0.46 L_{dv}=0.7 L_{dv}=0.83

Fig. 12 Comparison of void fraction contours in straight and curved ducts

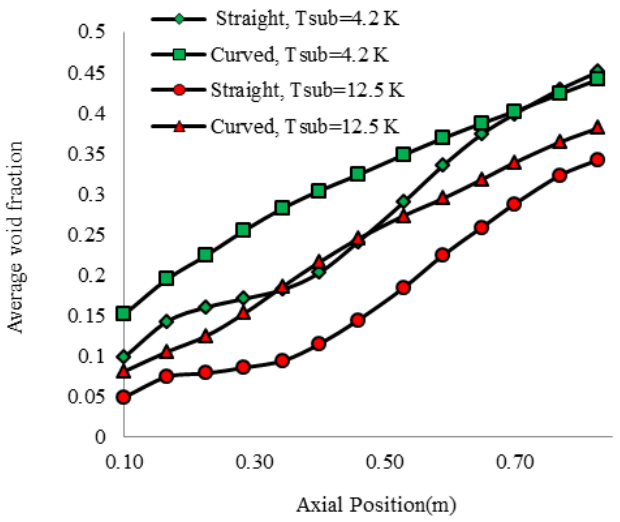

Fig. 13 Radially-averaged axial void fraction profile for comparison between straight and curved duct

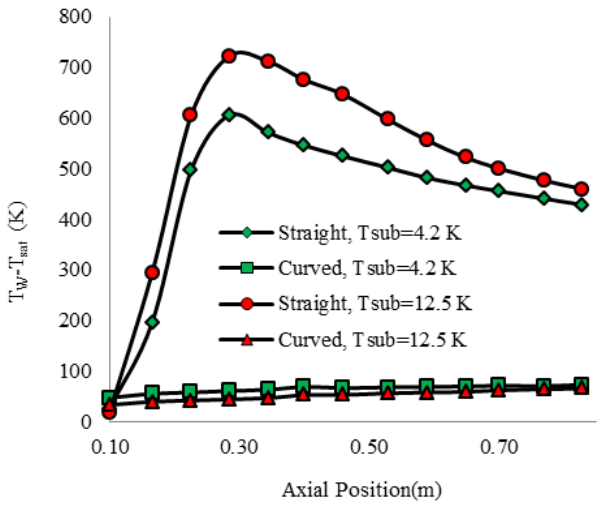

Fig. 14 Radially-averaged axial wall superheat profile for comparison between straight and curved duct

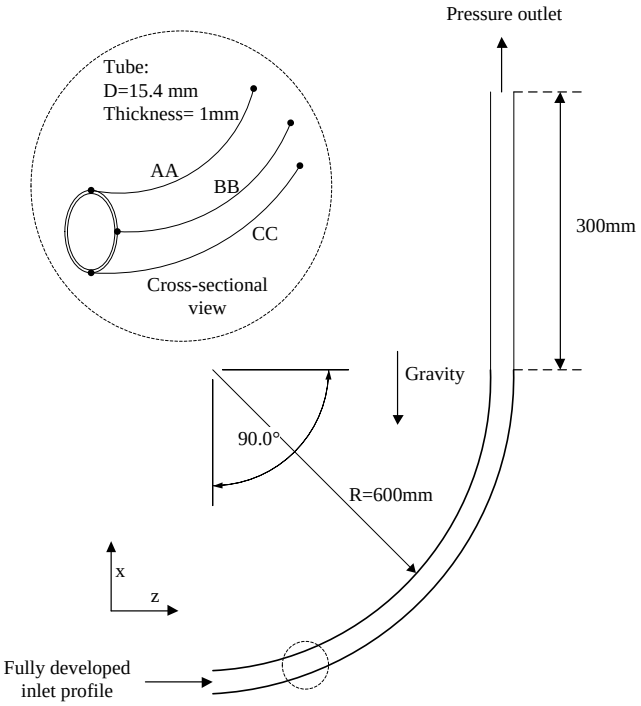

(a) Two-phase flow duct geometry

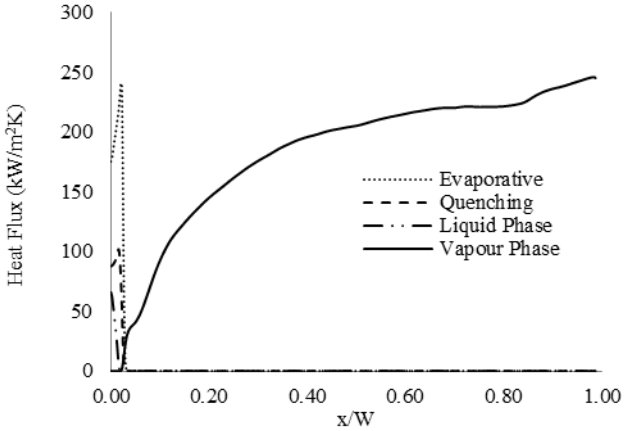

(c) Curved duct - Profile along AA (*inner wall*)

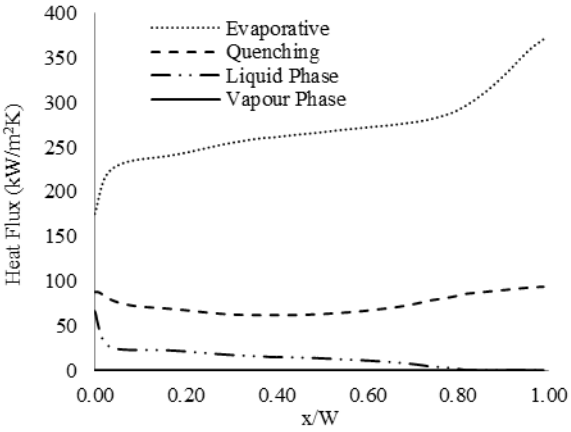

(d) Curved duct - Profile along BB *(side wall)*

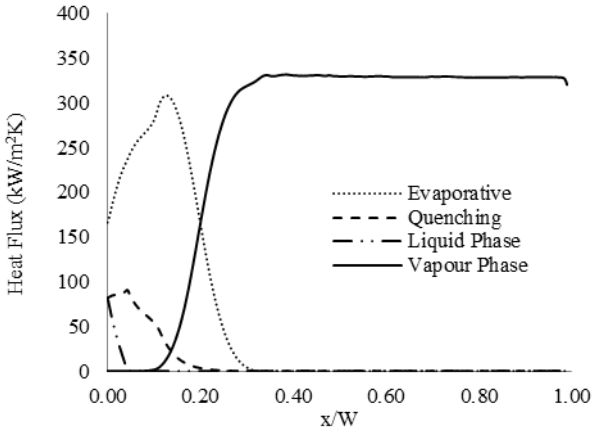

(b) Straight duct

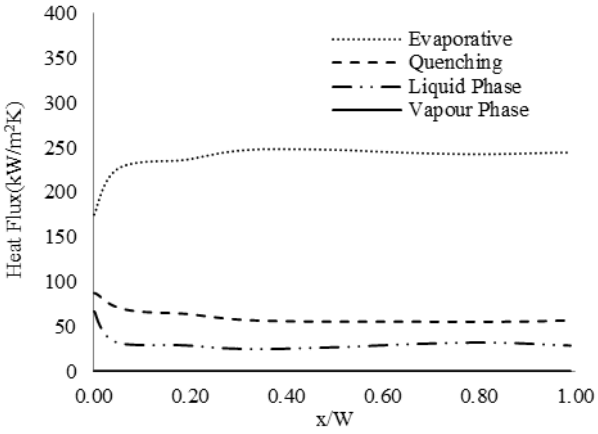

(e) Curved duct - Profile along CC *(outer wall)*

Fig. 15 Profiles of wall heat flux components used in simulation model with heat flux partitioning for straight and curved ducts